Vortex identification based on the Liutex method and its effect on fish passage upstream

Ruiguo Yang
Kunming University of Science and Technology
Chunying Shen (shenchunying520@163.com)
Kunming University of Science and Technology https://orcid.org/0000-0002-1008-4493
Xiaotao shi
China Three Gorges University
Mingming Wang
Shanghai Investigation Design and Research Institute
Shihua He
Kunming University of Science and Technology

Research Article

Keywords: Vertical Slit Fishway, vortex identification method, Liutex, Large Eddy Simulation (LES), fish experiment, Computational fluid dynamics

Posted Date: August 2nd, 2023

DOI: https://doi.org/10.21203/rs.3.rs-3204860/v1

Vortex identification based on the Liutex method and its effect on fish passage upstream

Journal of Hydrodynamics

Ruiguo Yang [1], Chunying Shen [1]*, Xiaotao Shi [2], Mingming Wang [1,3], Shihua He [1]

1. *Faculty of Electrical Power Engineering, Kunming University of Science and Technology, Kunming 650500, China*
2. *Hubei International Science and Technology Cooperation Base of Fish Passage, China Three Gorges University, Yichang 443002, China*
3. *Shanghai Investigation, Design & Research Institute Co., Lt，Shanghai 200434, China*
*Correspondence: Chunying Shen, E-mail address: shenchunying520@163.com

Abstract: Fishway research is important for mitigating the fragmentation of river habitats caused by hydraulic projects. The vertical slit fishway is a broadly used fishway type because of its high efficiency and adaptability to water levels. However, the resulting vortex current disrupts the fish passage hence directly affecting fish migration. This study aims to accurately capture the vortex structure in the fishway and analyze the effect of vortex elements (vortex structure, vortex intensity, etc.) on fish. We conducted an analysis of the three-dimensional current flow field in the fishway through the utilization of an experimental model and the Large Eddy Simulation (LES) method for dynamic stress. Moreover, we captured the vortex information in the fishway at different flow rates using the Liutex vortex identification method and investigated the effect of the vortex on fish migration. The results revealed that the structures inside the fishway pool occupy most of the room; however, the areas with higher vortex strength were primarily located in the vortex near the vertical seam and the mainstream; the vortex strength inside the fishway gradually increases with increasing flow, suppressing fish migration. Fish experienced significantly increased resistance when encountering strong vortexes. This suggests that the vortex may act as a physical barrier to fish migration. These findings highlight the potential negative effects of vortex on fish movement and reiterate the importance of understanding vortex dynamics for aquatic environmental management. As an effective tool for identifying vortexes in fluid flow, the Liutex method demonstrates features of vortex within the fishway, thereby providing important insights into the interaction between fluid dynamics and aquatic organisms.

Keywords：Vertical Slit Fishway; vortex identification method; Liutex; Large Eddy Simulation (LES); fish experiment; Computational fluid dynamics

0.Introduction

With the use and development of river water resources, dams have been or are being built in most rivers [1,2]. Dam construction has had a significant effect on the river ecosystem, particularly their barrier effect on the river, which directly blocks the upstream and downstream fish passage and affects the

normal two-way spread of fish communities between habitats [3]. A fishway is a hydraulic structure that allows certain fish species to migrate upstream and downstream in a river amidst natural and man-made barriers [4]. Fishway can be classified as Daniel, vertical slot, pool weir, imitation natural fishways, etc. Among them, Vertical Slit Fishway is broadly used across the globe for its good operation under a wide range of water level conditions and high fish passage efficiency.

The water flow in the vertical slit fishway forms a jet at the vertical slit, creating a circulation area on both sides of the mainstream [5]. Notably, the circulation area inside the pool room is an important factor affecting fish passage. Nikora et al. [6] reported that the effect of the eddy on fish may be associated with the size of the eddy and that of the fish. Lupandin [7] used the one-dimensional time dependence of flow velocity to determine the scale of turbulence (L) and utilized L to represent the mean vortex size. They found that the vortex size and fish size influence the swimming performance. Besides, the torque generated by the vortex hydrodynamics makes the fish prone to tipping over; therefore, the fish need to use their pectoral fins to regain their balance, thus increasing their hydrodynamic resistance. Marriner et al [8] used vorticity magnitudes to analyze vortices in the resting pool of the fishway and discovered that vortices delay or prevent fish passage. Zhao et al. [9] observed the 3D vortex structure within the conventional and modified fishways based on large eddy simulations using a Q-criterion with a larger threshold.

Several studies have provided evidence of the substantial impact of vortex on fish passage in fishways, and previous research focused on the vortex in fishway pairs. However, other studies characterized the vortex structure only by velocity vectors, vortex volumes, or average streamlines, successfully capturing limited vortex information. With the advancement of vortex identification technology, recent studies have introduced a third-generation vortex identification method known as Liutex [10]. The Liutex method mathematically extracts the rigid rotating part of the fluid motion, thereby defining and visualizing the vortex [11]. The Liutex method is superior to the previous vortex identification methods. The major benefit of the Liutex isosurface method is that it does not contain shear or tensile contamination [12]. The Liutex method represents the rotation or vortex intensity of the fluid, which is more valuable than previous methods that could not measure the rotation or vortex intensity of the fluid [13-15]. Therefore, the Liutex method has also been broadly used in the field of fluid mechanics [16-18].

The three-dimensional computational fluid dynamics (CFD) model is an effective tool to analyze the flow field of a vertical slit fishway. The flow field in a vertical slit fishway has a complex turbulent structure, and previous studies have commonly used the RNG k-ε and LES methods to analyze the turbulence in the fishway. Fuentes-Pérez et al. [19] observed that both the LES and RNG turbulence models yielded satisfactory outcomes. Nonetheless, the LES approach was more spatially consistent with the measured data, making it particularly relevant for biological studies focusing on smaller spatial and temporal scales. Quaresma et al. [20] compared four methods, RNG k-ε, k-ε, k-ω, and LES, and noted that LES corresponds with the experimental results. Elsewhere, Santos et al [21] revealed that the LES is slightly better than the RNG method in capturing turbulence values.

The VOF method has shown to be effective in accurately capturing free water surfaces, and several studies have successfully utilized the VOF method to model the free surface of fishways with favorable outcomes [22,23]. To more accurately study the vortex information in the fishway, this work constructed the fishway model based on the aqueduct and measured the instantaneous flow velocities at the characteristic points of the model using a 3D Acoustic Doppler Velocimeter (ADV). Furthermore, the 3D flow field of the vertical slit fish passage was simulated using the LES and VOF methods. The vortex structure inside the fishway was also captured using the Liutex method, and the vortex characteristics inside the fishway pond were analyzed under different water flow conditions. Eventually, the fish experiments were performed to investigate the effect of vortex characteristics inside the fishway pond on fish upstream.

1. Materials and Methods

1.1 Experimental Steps and Procedures

As shown in Figure 1, a scale model of a vertical slit fishway was constructed on the flume. The model was constructed in a glass flume 7.5m long, 0.3m wide, and 0.5m high. The fishway was flanked by the side walls of the flume, and the bottom slope and baffle comprised Plexiglas. The model was built in a 7.5m long, 0.3m wide, and 0.5m high glass flume, the two sides of the model were the side walls of the flume, and the bottom slope and baffle were made of acrylic panels. The flow in the fishway was controlled by a gate valve at the front of the flume and the whole structure was in the water flow circuit.

The model had five levels of pool chambers with a 3% bottom slope and a 10:8 ratio of length to width of the chambers. The model inlet front length was long with smooth model inlet water flow. The flow velocity of the experiment was measured using a 3D Doppler velocimeter (ADV), which determines instantaneous flow velocity in the X, Y, and Z directions at a given point. The ADV was mounted on a trolley on top of the flume, which could measure the three-dimensional flow velocity at the target point by freely adjusting the horizontal and vertical distances. The ADV fixed by the trolley reduces the measurement error and increases the accuracy of the experiment.

To analyze the vortex characteristics of the fishway under different current conditions, dimensionless variables Q^* [24] were used to characterize the different water flow conditions. Q^* is defined as follows:

$$Q^* = \frac{Q}{\sqrt{gS_0}b^{\frac{5}{2}}} \tag{1}$$

Where Q denotes the flow rate, g denotes the acceleration of gravity, S_0 denotes the bottom slope of the fishway, and b denotes the net width of the fishway. The Q^* values corresponding to the three different water flow conditions were calculated to be 0.095, 0.166, and 0.261, respectively.

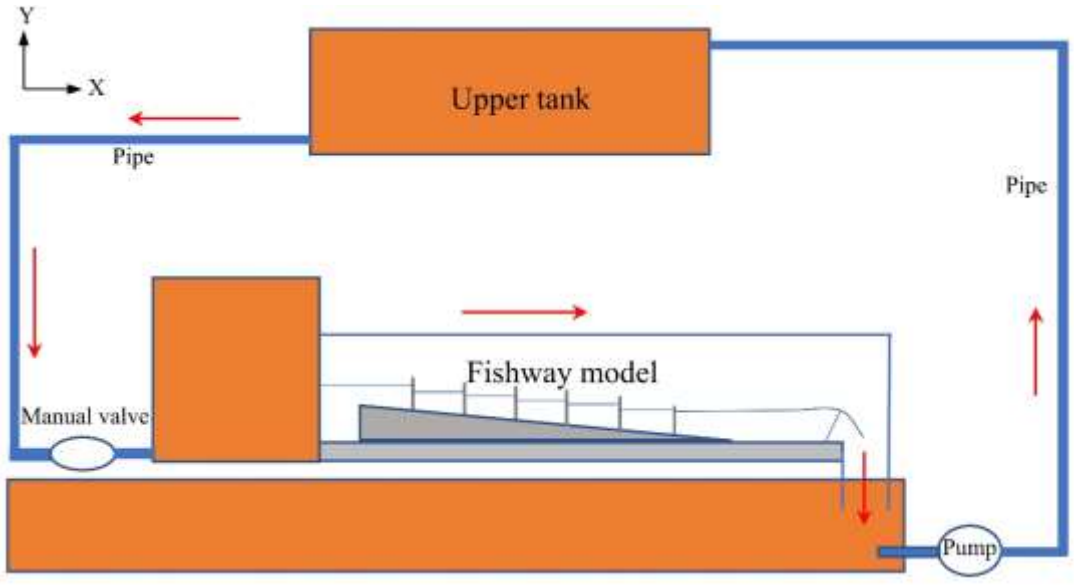

Fig. 1 Fish passage model installation schematic.

1.2 Numerical model

The numerical simulation model was developed based on the physical experimental model. In this study, the coordinate system had its origin situated at the lower left corner of the inlet. The X-axis was

aligned parallel to the direction of water flow, the Y-axis was perpendicular to the bottom, and the Z-axis was transverse to the water flow direction. The components of velocity, namely *u*, *v*, and *w*, corresponded to the velocities in the X, Y, and Z-axis directions, respectively. The model used a mixed mesh of tetrahedra and hexahedra to profile the fluid domain (Figure 2). The model pool was 0.625 m long, with an inlet section of 2.375 m and an outlet section of 1.5 m. The three-dimensional computational fluid dynamics (CFD) solver FLUENT was to simulate the distribution of flow fields in the fishway. The LES turbulence model was utilized to calculate the turbulence characteristics within the vertical slot.

The bottom, side walls, and partitions of the fishway were considered as solid boundaries with no-slip boundary conditions. The upper part of the model was defined as a pressure boundary condition, with a relative pressure of zero. The near-wall viscous layer was handled using the wall function method, while the conventional wall boundary conditions were applied to the walls and baffles throughout the fishway. The velocity inlet boundary conditions were used for the model inlet, and the velocity values were determined by experimental velocity. The inlet velocity values corresponding to the three different sets of water flow conditions were u = 0.069 m/s, u= 0.081 m/s, and u = 0.092 m/s. Pressure-type exit boundary conditions were provided at the exit of the model. The convergent solution was determined by running 40,000-time steps with a time step of 0.001s to achieve it.

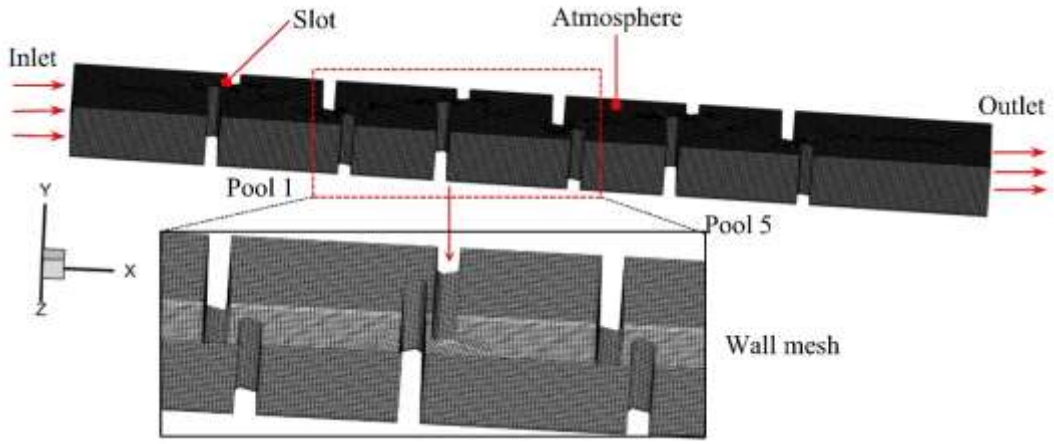

Fig. 2 Model geometry and meshing diagram.

The LES method was employed to simulate the three-dimensional turbulent flow field in the fishway. The simulation used the PISO algorithm for solving the equations, the momentum equation was discretized using the second-order upwind, and the time term was discretized using the second-order implicit method. In turbulent large eddy simulations, a filter function was first used to decompose the

127 flow variable $f(x, t)$ into large-scale quantity $\bar{f}(x,t)$ and small-scale quantity $f'(x,t)$.

$$f(x,t)=\bar{f}(x,t)+f'(x,t) \tag{2}$$

128 Substituting equation (2) into the Navier-Stokes equation and the continuity equation to obtain the
129 control equation for the large eddy simulation

$$\frac{\partial \rho}{\partial t}+\frac{\partial}{\partial x_i}(\rho\bar{u}_i)=0 \tag{3}$$

$$\frac{\partial}{\partial t}(\rho\bar{u}_i)+\frac{\partial}{\partial x_j}(\rho\bar{u}_i\bar{u}_j)=\frac{\partial}{\partial x_j}(\mu\frac{\partial \sigma_{ij}}{\partial x_j})-\frac{\partial \bar{p}}{\partial x_i}-\rho\frac{\partial \tau_{ij}}{\partial x_j} \tag{4}$$

130 Where i、j=1、2、3，σ_{ij} is the stress tensor around the molecular viscosity, τ_{ij} is subgrid-scale stress
131 (SGS).

132 The subgrid-scale model uses the basic Smagorinsky model, and the SGS equation expression [25]
133 is：

$$\tau_{ij}-\frac{1}{3}\tau_{kk}\delta_{ij}=-2\mu_t\bar{S}_{ij}=-2c_s^2\Delta^2|\bar{s}|\overline{s_{ij}} \tag{5}$$

134 Where δ_{ij} is the Kronecker δ function, μ_t is the sublattice scale vortex viscosity coefficient，Δ
135 Indicates the filter width, $|\bar{S}|=\sqrt{2\bar{S}_{ij}\bar{S}_{ij}}$ is the mode of the strain rate tensor. The expression of $\bar{S}_{ij}$
136 is given by：

$$\bar{S}_{ij}=\frac{1}{2}\left(\frac{\partial \bar{u}_i}{\partial x_j}+\frac{\partial \bar{u}_j}{\partial x_i}\right) \tag{6}$$

137 The Volume of Fluid (VOF) method was utilized to track the free surface and analyze the fluid
138 behavior. The fluid-to-grid volume ratio function F was examined in each grid cell to determine the
139 variation of the fluid. The volume of fluid method (VOF) equation proposed by Hirt and Nichols [26] is
140 as follows:

$$\frac{\partial \alpha_w}{\partial t}+u_i\frac{\partial \alpha_w}{\partial x_i}=0 \tag{7}$$

141 Where $\alpha_w=0$ means that there is no water in the calculation cell, $\alpha_w=1$ means that the calculation
142 cell is all water, $0<\alpha_w<1$ indicates that the calculation cell is a mixed interface of water and air and

there is a cross interface.

1.3 Model Validity

No truly grid-independent scheme exists for large eddy mode simulations [19], but Celik [27] proposed a criterion that a good LES model should resolve at least 80% of the total turbulent kinetic energy. To perform the analysis and select the best resolution, different grid resolutions were compared and the grid with LES IQ greater than 0.80 was finally selected for calculation (the number of grids was 201825，316043，437056 respectively).

To confirm the validity of the model, the water depth and velocity in the X-direction of each cell in the simulation results were compared with experimental results under the current condition of Q^*=0.09. The simulated free water surface was obtained by the VOF method, and the experimental water depth values were obtained by averaging multiple sets of measurements. The water depths of the simulated results and the experimental results matched, as shown in Figure 3(a). The experimental flow velocities were measured by ADV, and the water depths within the five pool chambers and the flow velocities in the X-flow direction at the outlet of the vertical slit of the five pool chambers were monitored under similar flow conditions. The experimental data were compared and analyzed with the simulated data, and the numerical simulations were consistent with acceptable accuracy despite errors in the experimental data (Fig. 3 (b)).

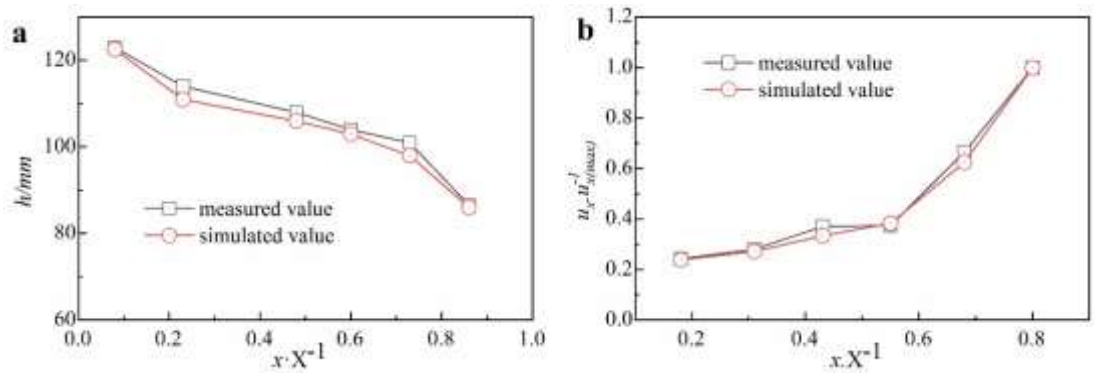

Fig. 3 Comparison of simulation and experimental results. (a) Water depth in the center of the pool chamber of each fishway; (b) velocity in the x-direction at the characteristic point of the centerline of the fishway.

1.4 Vortex identification method

The vortex structure in the fishway is a complex water flow structure. Herein, the Liutex method

was used to capture the vortex structure in the vertical slit fishway. Liutex represents the rigid rotating part of the fluid motion [28-31]. The vector *R* is defined as follows:

$$R = \begin{cases} 2(\beta - \alpha), & \alpha^2 - \beta^2 < 0 \\ 0, & \alpha^2 - \beta^2 \geq 0 \end{cases} \tag{8}$$

Where α and β are denoted as

$$\alpha = \frac{1}{2}\sqrt{\left(\frac{\partial v_Q}{\partial y_Q} - \frac{\partial u_Q}{\partial x_Q}\right)^2 + \left(\frac{\partial v_Q}{\partial y_Q} + \frac{\partial u_Q}{\partial x_Q}\right)^2} \tag{9}$$

$$\beta = \frac{1}{2}\left(\frac{\partial v_Q}{\partial x_Q} - \frac{\partial u_Q}{\partial y_Q}\right) \tag{10}$$

Where x_Q、y_Q are the variables generated in the initial *xyz* coordinate system using *Q* rotation，v_Q and u_Q are the velocity components in the $x_Q y_Q z_Q$ coordinate system after rotation.

2. Results

In this study, the three-dimensional flow field inside the fishway was simulated by large eddy simulation based on experiments. The Liutex method was used to capture the three-dimensional vortex structure inside the fishway pond under different flow conditions separately. The relationship between fluid vortex dynamics and aquatic organisms was investigated through fish experiments to reveal the vortex effect in the fishway on fish migration.

2.1 3D vortex structure in the Fishway

As shown in Figure 4(a), a large vortex and a small vortex were formed on both sides of the mainstream as the water flowed downstream from the vertical slit position in the upper pool chamber. As water flows downstream from the vertical slit position in pool chamber 1, the flow becomes biased toward the left side wall, and a small portion of the water flow near the side wall changes direction, creating a smaller corner vortex at the corner position. The main flow then flows downstream along the left-hand side wall, and upon reaching the next vertical seam position, a portion of the left-hand side changes direction and flows into the right-hand side of the area. The flow velocity in the right side area is smaller than that in the main flow area, and the backward-flowing water forms a larger backflow area

in this right side area. The water flow in the return area rotates with the vortex, and part of the peripheral water flow meets the main flow again and flows into the main flow to the next level of the pool chamber. Smaller-scale vortex structures also exist at the vertical seam location (Figure 4(b)). When the water flows through the vertical slit position, two smaller-scale vortex structures are formed around the side walls on both sides of the vertical slit.

Since the capacity to capture vortex information is limited, only the approximate location of the vortex surface can be roughly obtained through the experiment, and it is difficult to obtain a characterization of the bottom vortex structure and vortex intensity analysis through the experiment. Therefore, this study used the Liutex vortex identification technique to capture the 3D vortex structure in the fishway and analyzed its information.

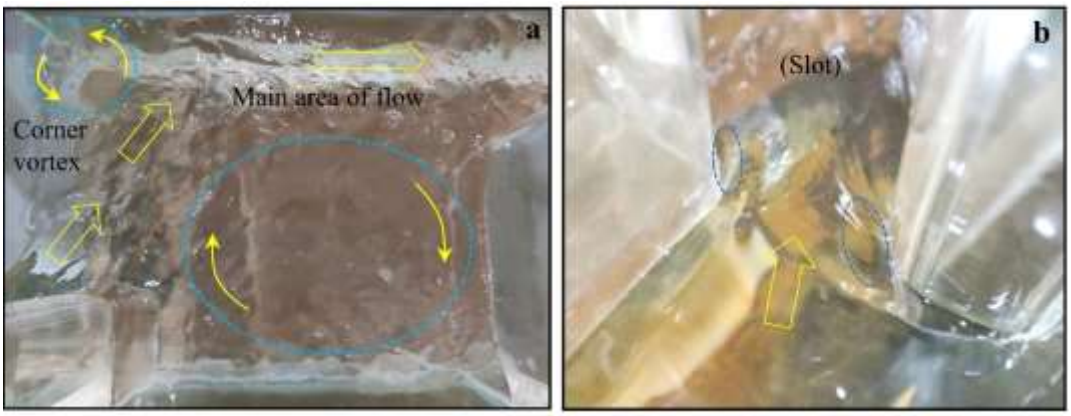

Fig. 4 Vortices on the surface of the water flow. (a) at the pool chamber; (b) at the vertical seam position. (Arrows indicate the direction of water flow and vortex)

Figure 5 illustrates the 3D vortex structure of pool chamber 1 captured using the Liutex method with different thresholds at a Q^*=0.095 water flow condition. The vortex structures captured in the cell using the threshold |Rortex| = 0.1 are not only the larger-scale vortex structures in the pool but also some small-scale broken vortex structures. The large-sized vortex on the left and the vortex at the right corner occupies nearly most of the pool, which is consistent with experimental observations. The diameter of the large-scale vortex surface on the left side was larger than the middle and bottom of the flow, and the left and right sides of the vortex were interconnected at the exit of the vertical slit. When the water returning from the surface of the flow reaches the outlet of the vertical slit, this part of the flow merges into the main stream, for vortex structure formation. Specifically, previous studies focused more on the

horizontal vortex in the pool; however, the three-dimensional structure of the vortex captured by the Liutex method is more intuitive. Besides, the three-dimensional vortex node in the return region of the fishway pool is not a regular geometry but comprises multiple irregular vortex structures.

The Liutex method also captured the vortex structure at the slot position in the fishway. The vortex at the vertical slit was in the shape of a regular semi-cylinder against the side walls of the baffle on both sides of the slot, and the corresponding vortex was generated at both the left and right sides of the slot. When the water flow in the fishway passes through the slot, the direction of the water flow changes, thereby forming a corresponding vortex structure at the slot position.

When the Liutex method with threshold |Rortex| = 1 is used to capture the vortex structure in the fishway, the size of the captured vortex structure is significantly reduced, the broken vortex structure is reduced, and the 3D vortex structure is presented. The vortex structure captured on the right side of the pool is the vertical axis vortex at the corner, at the same time capturing the vortex at the slot position. Although the Liutex method with a small threshold can capture more vortex structures, we analyzed major vortex structure characteristics within the pool; therefore, a threshold of |Rortex| = 1 may help in analyzing the vortex structure characteristics.

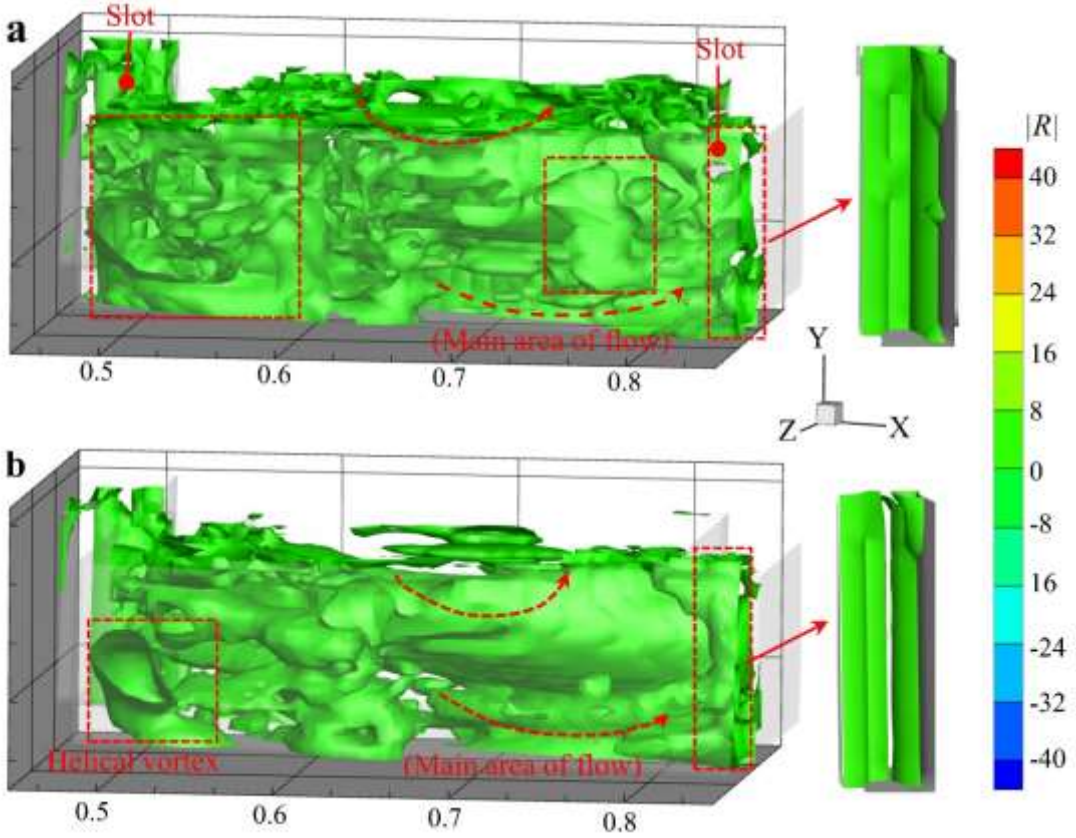

Fig. 5 (a) Iso-surfaces of |Rortex| = 0.1, colored by Rortex; (b) Iso-surfaces of |Rortex| = 1, colored by Rortex, Q^*=0.095. (Arrows indicate the direction of water flow and vortex)

The effect of different water flow conditions on the vortex characteristics within the pool was investigated by varying the flow rate in the fishway. Based on Q*=0.095, we compared and analyzed the three-dimensional vortex structure characteristics inside the lower fishway with different flow conditions of Q*=0.166 and Q*=0.261.

As shown in Fig. 6, the three-dimensional vortex structure in pool 1 captured by Liutex was similar for the flow conditions of Q*=0.166 and Q*=0.261, and the vortex size in the fishway increased with increasing Q*. The effect of changing Q* on the three-dimensional vortex structure in the fishway was small, indicating that under different flow conditions, the vortex in the pool chamber majorly comprised large-size vortices in the return region. This indicates that under different water flow conditions, the vortex inside the pool primarily consists of large-size vortices in the return area, corner vortices at the corners, and vertical axis vortexes at slot position. The three-dimensional vortex structure in the fishway was not a regular geometric structure except for the slot position, and the vortex structure inside the pool had a larger vortex diameter in the area near the surface of the flow and a smaller vortex diameter in the area via the bottom of the flow.

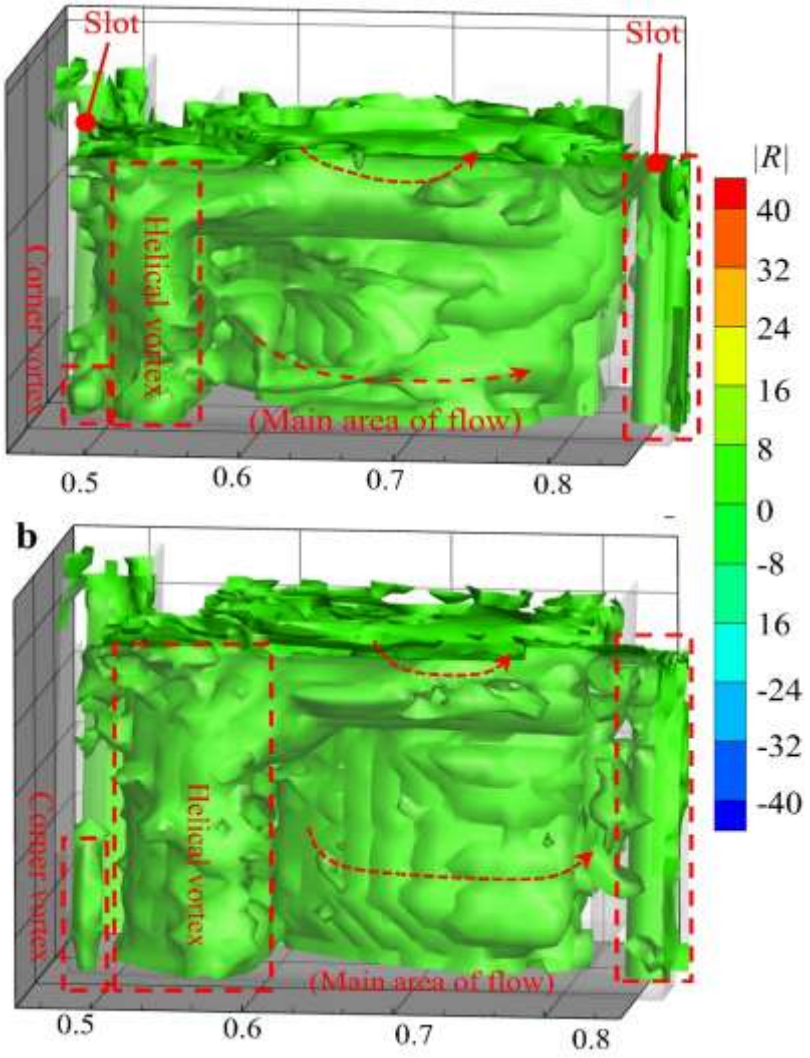

Fig. 6 Iso-surfaces of |Rortex| = 0.1, colored by Rortex. (a) Q^*=0.166; (b) Q^*=0.261. (Arrows indicate the direction of vortex water flow and)

2.2 Vortex characteristics inside the pool

For more vortex information, we compared the rotation intensity within the fishway under three water flow conditions separately. Figure 7 shows the distribution of the fish channel vortex rotation intensity. Vortex at the location of the slot in the fishway > Large-scale vortex > Angular vortex. Among them, the vortex at the slot had the vortex at two positions of the large baffle and the small baffle, and the intensity of the vortex generated at the large baffle position was greater than that at the small baffle position. The slot position of the fish passage had a concentrated water flow and high velocity, generating largest vortex intensity in this position (strong vortex region $|R| > 10$). Since the large baffle is located before the small baffle, water flowing through the slot contacts the side wall of the large baffle first, and

the vortex intensity at the location of the large baffle becomes greater than that at the location of the small baffle. The large-scale vortex intensity in the return flow area was majorly located in the nearby area near the mainstream.

The area with the greatest vortex intensity within the fishway pool was located in pool 5, with a significantly greater vortex intensity than the other pool, and the area with a vortex intensity greater than 10 occupies approximately 10% of the pool. At the exit of the fishway, there was also a region with high vortex intensity.

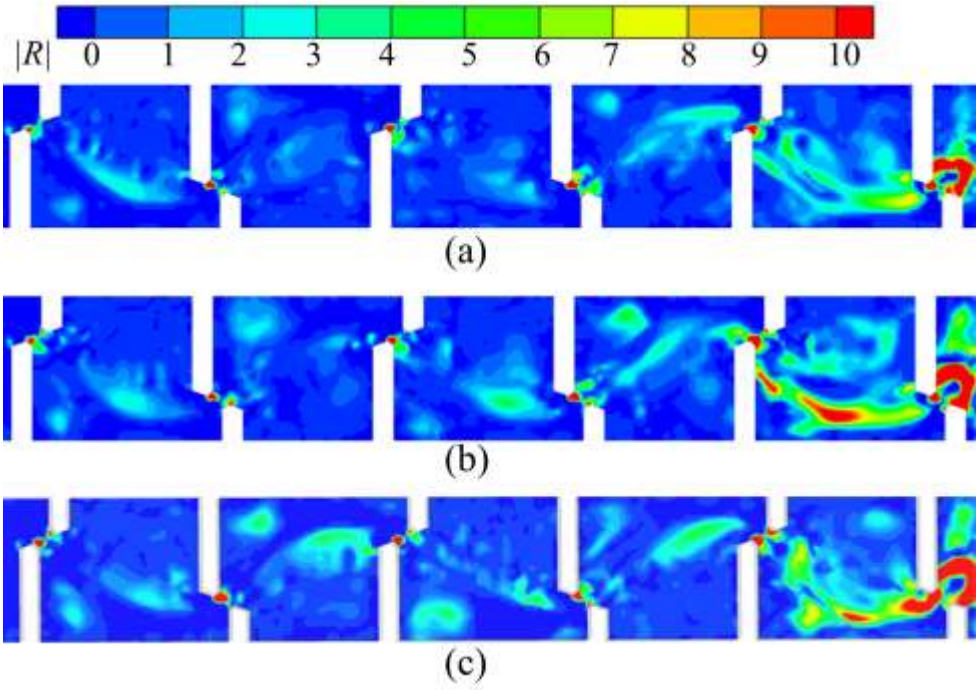

Fig. 7 Vortex rotation intensity (a) Q^*=0.095;(b) Q^*=0.166; (c) Q^*=0.261.

There is a clear difference in the intensity of the vortex inside the pool under different water flow conditions. In the downstream direction, the slot is numbered separately, the slot at the inlet of pool 1 is defined as slot 1, and the slot at the outlet position of pool 5 is defined as slot 6. Figure 8 shows the maximum rotational intensity of the vortex generated at the vertical seam positions under three different sets of water flow conditions. The rotation intensity of the vortex gradually increased with increasing Q*.

Under different water flow conditions, with the backward movement of the water flow, no obvious linear change relationship was noted between the strength of the slot locations. The vortex intensity of the vertical seams near the left side wall (slot 1, slot 3, slot 5) and near the right side wall (slot 2, slot 4, slot 6) were analyzed, and that of both the left vertical seam and the right vertical seam in the fishway gradually increased. Overall, the intensity of the vortex generated by the left vertical seam was greater than that of the right vortex.

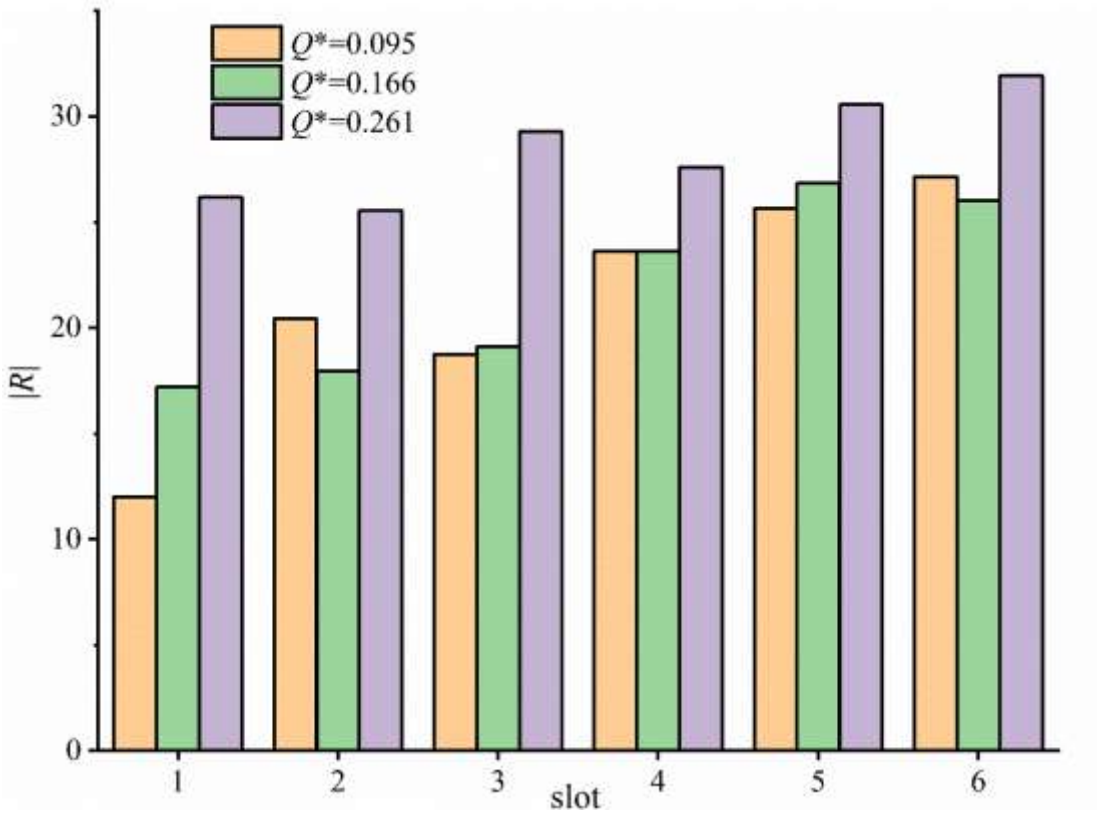

Fig. 8 The maximum rotational intensity of the vortex at the vertical seam position.

2.3 Effects of the Vortex on fish migration

An experimental study was conducted using 13-20 cm Crawfish to study the effect of vortex in the fishway on fish migration. In the experiment, the fish followed the mainstream from one slot through the pool to the next level of slot and chose the most central position up the slot location during the migration process (Figure 9). Based on the above vortex intensity analysis at the vertical seam, the closer the vertical seam location of the side walls on both sides, the greater the vortex intensity. Although the intensity of the vortex at the slot location is significant, if the fish do not pass through the vortex area at the vertical slot location, the effect of the vortex at the vertical slot location on the fish upstream becomes extremely limited. The tendency of fish to avoid areas with higher vortex intensity suggests that vortex may block fish migration. During fish migration, the body prefers the bottom position of the current, with fewer areas of the vortex at the bottom and lower vortex intensity in the return region, reducing the effect of the vortex on fish migration and optimizing the choice of bottom migration.

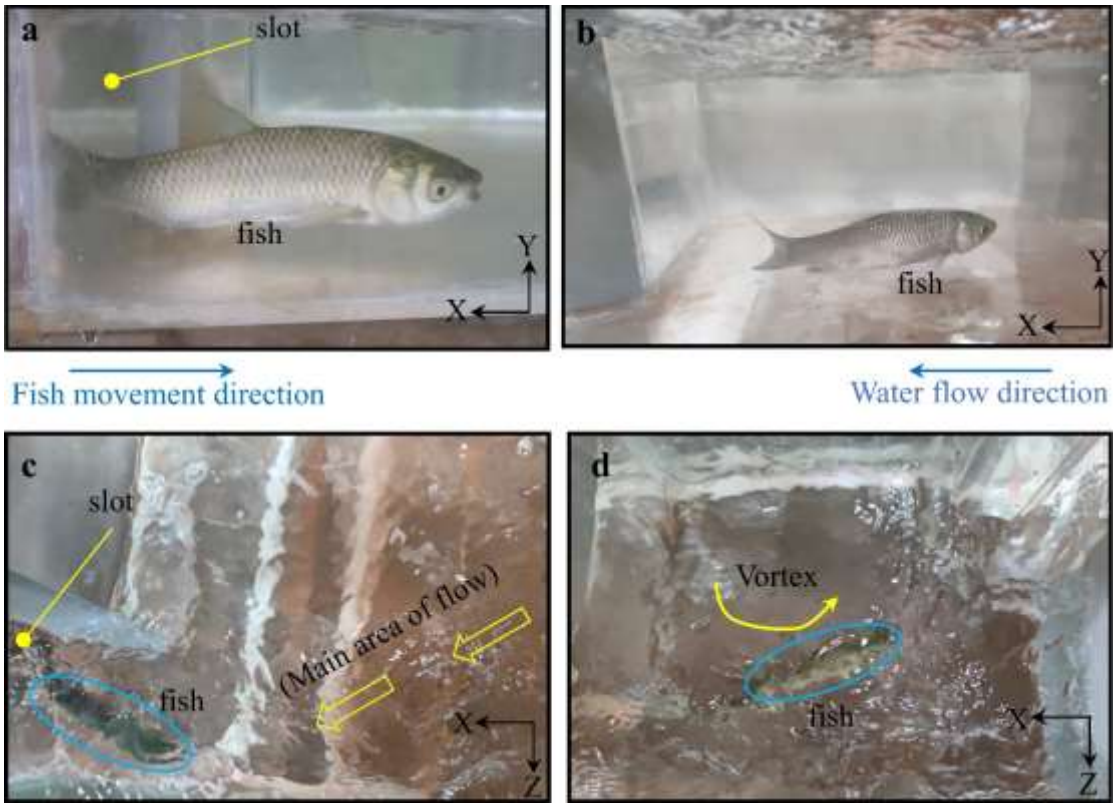

Fig. 9 Fish migration experiment under Q^*=0.095 current conditions. (Arrows indicate the direction of vortex water flow and vortex)

Although the large-scale vortex in the reflux zone occupies most of the pool, its effect on fish migration is limited. After reaching the next level of the pool, the fish did not first swim to the migratory zone with low flow velocity but swim along the mainstream to the next level of the pool. However, due to the decrease in physical strength, a few fish were unable to reach the next level of the pool through the slot and eventually swam to the center of the large-scale eddy in the reflux area. The vortex intensity on the back side of the large-scale vortex from the mainstream was small, yet beneficial to the fish despite the large vortex diameter. The fish recovered their physical strength in this region before attempting to reach the next level of the slot.

Fish migration became difficult with Q^* increase. Under a higher flow rate, the vortex intensity in the fishway also increased. As shown in Figure 10, the fish would passively enter the reflux zone when they could not reach the next level of the pool through the slot, and most of the fish would gradually get lost in the vortex while swimming in the reflux zone. Therefore, a small flow rate meeting fish passage ensures smooth fish migration in the fishway.

Fig. 10 Q^*=0.261 Fish migration experiment under Q*=0.261 flow conditions. (Arrows indicate the direction of vortex water flow and vortex)

3. Conclusions

In the study, we constructed an experimental model of the fishway to investigate the vortex features within the fishway and their impact on fish migration. Additionally, a combination of large eddy simulation (LES) and Volume of Fluid (VOF) methods was employed to simulate the three-dimensional flow patterns within the fishway. The grid independence of LES was evaluated using the IQ index, and the simulation results were compared to the experimental data obtained from an acoustic Doppler velocimeter (ADV), yielding satisfactory accuracy for the model. Based on the numerical simulations, the Liutex method was applied to capture the 3D vortex structure within the fishway under different water flow conditions. Furthermore, we analyzed the characteristics of the 3D vortex structure and the intensity of vortex rotation in the fishway. Through fish experiments, we explored the influence of the vortex within the fishway on fish migration. The following conclusions were drawn from our study:

(1) The vortex in the fishway comprised a large-size vortex in the return area, a corner vortex at the corner, and a vertical axis vortex at the vertical slit position. Vortex diameter inside the pool near the surface of the water flow was significantly larger than that of the vortex near the bottom of the water flow.

(2) The vortex intensity was greatest at the location of the slot of the fishway and the outlet of the fishway, and the angular vortex intensity was least at the corner location of the pool. The areas with higher vortex intensity were primarily distributed near the mainstream despite the large-scale vortex in the return flow area occupying most of the pool.

(3) Vortex can be a physical barrier to fish migration, and fish tend to avoid areas of higher vortex strength during migration.

(4) The vortex effect on fish is majorly attributed to vortex intensity. As Q^* increases, the vortex strength also gradually increases, making fish migration more difficult. Therefore, the use of low flows is helpful for fish migration when fish passage is guaranteed.

Acknowledgements

This study used the LiutexUTA code developed by Chaoqun Liu at the University of Texas at Arlington. This work was supported by the National Natural Science Foundation of China (Grant numbers 52069009 and 51369013).

Statements and Declarations

The authors declare that they have no known competing financial interests or personal relationships that could have appeared to influence the work reported in this paper.

Author Contributions

Ruiguo Yang: Conceptualization, Methodology, Formal analysis, Writing-Original Draft. **Chunying Shen**: Conceptualization, Methodology, Writing-Original Draft, Funding acquisition. **Xiaotao Shi**：Conceptualization, Visualization, Review. **Mingming Wang**：Investigation, Formal analysis. **Shihua He**：Investigation, Formal analysis，Funding acquisition.

Funding

This research was funded by the National Natural Science Foundation of China (Grant numbers 52069009 and 51369013).

Conflict of interest:

All authors declare no conflict of interest.

References

[1] Nilsson, C. Fragmentation and Flow Regulation of the World's Large River Systems[J]. *Science*, 2005,308(5720), 405-408.

[2] Zarfl, C., Lumsdon, A. E., Berlekamp, J.et al. A global boom in hydropower dam construction [J]. *Aquatic Sciences*, 2015, 77(1), 161-170.

[3] Radinger, J., Wolter, C.Patterns and predictors of fish dispersal in rivers [J]. *Fish and Fisheries*, 2014,15(3), 456-473. https://doi.org/10.1111/faf.12028

[4] Boiten, W. Flow measurement structures[J]. *Flow Measurement & Instrumentation*, 2002,13(5-6), 203-207.

[5] Rajaratnam, N., Gary, V., Katopodis, C. Hydraulics of Vertical Slot Fishways [J]. *Journal of Hydraulic Engineering*, 1986, 112(10), 909-927.

[6] Nikora, V. I., Aberle, J., Biggs, B., J. et al. Effects of fish size, time-to-fatigue and turbulence on swimming performance: a case study of Galaxias maculatus [J]. *Journal of Fish Biology*, 2010, 63(6), 1365-1382.

[7] Lupandin, A. Effect of flow turbulence on swimming speed of fish [J]. *Biology Bulletin*, 2005,32, 461-466.

[8] Marriner, B. A., Baki, A. B. M., Zhu, D. Z. et al. Field and numerical assessment of turning pool hydraulics in a vertical slot fishway [J]. *Ecological Engineering*, 2014, 63, 88-101.

[9] Zhao, H., Xu, Y., Lu, Y. et al. Numerical Study of Vertical Slot Fishway Flow with Supplementary Cylinders [J]. *Water*, 2022, 14(11). https://doi.org/10.3390/w14111772

[10] Dong, X., Gao, Y., Liu, C. New normalized Rortex/vortex identification method [J]. *Physics of Fluids*, 2019, 31(1). https://doi.org/10.1063/1.5066016

[11] Wang, Y.-q., Gao, Y.-s., Xu, H. et al. Liutex theoretical system and six core elements of vortex identification[J]. *Journal of Hydrodynamics*, 2020, 32(2), 197-211. https://doi.org/10.1007/s42241-020-0018-0

[12] Gao, Y., Liu, C. Rortex and comparison with eigenvalue-based vortex identification criteria [J]. *Physics of Fluids*, 2018, 30(8). https://doi.org/10.1063/1.5040112

[13] Yu, C. Investigation of correlation between vorticity, Q, lambda(ci), lambda(2), Delta and Liutex [J]. *Computers & Fluids*, 2021,225(1).

[14] Wu, Y., Zhang, W., Wang, Y. et al. Energy dissipation analysis based on velocity gradient tensor decomposition [J]. *Physics of Fluids*, 2020.32(3).

[15] Gui, N., Qi, H.-b., Ge, L. et al. Analysis and correlation of fluid acceleration with vorticity and Liutex (Rortex) in swirling jets [J]. *Journal of Hydrodynamics*, 2019, 31(5), 864-872. https://doi.org/10.1007/s42241-019-0044-y

[16] Shen, C.-y., Yang, R.-g., Qing, S. et al. Vortex analysis of water flow through gates by different vortex identification methods[J]. *Journal of Hydrodynamics*, 2023, 35(1), 112-124. https://doi.org/10.1007/s42241-023-0006-2

[17] Zhang, Z., Dong, S., Jin, R. et al. Vortex characteristics of a gas cyclone determined with different vortex identification methods [J]. *Powder Technology*, 2022, 404. https://doi.org/10.1016/j.powtec.2022.117370

[18] Shen, C., Yang, R., Wang, M. et al. Application of Vortex Identification Methods in Vertical Slit Fishways [J]. *Water*, 2023,15(11), 2053

[19] Fuentes-Pérez, J. F., Silva, A. T., Tuhtan, J. A. et al. 3D modelling of non-uniform and turbulent flow in vertical slot fishways [J]. *Environmental Modelling & Software*, 2018, 99, 156-169. https://doi.org/10.1016/j.envsoft.2017.09.011

[20] Quaresma, A., Pinheiro, A. Modelling of Pool-Type Fishways Flows: Efficiency and Scale Effects Assessment [J]. *Water*, 2021,13(6). https://doi.org/10.3390/w13060851

[21] Santos, H. A., Pinheiro, A. P., Mendes, L. et al. Turbulent Flow in a Central Vertical Slot Fishway:

Numerical Assessment with RANS and LES Schemes [J]. *Journal of Irrigation and Drainage Engineering(7)*, 2022,148.

[22] Stamou, A. I., Mitsopoulos, G., Rutschmann, P. et al. Verification of a 3D CFD model for vertical slot fish-passes [J]. *Environmental Fluid Mechanics*, 2018, 18(6), 1435-1461. https://doi.org/10.1007/s10652-018-9602-z

[23] Barton, A. F., Keller, R. J. 3D FREE SURFACE MODEL FOR A VERTICAL SLOT FISHWAY [J]. *IAHR congress* ,2003.

[24] Rajaratnam, N., Katopodis, C. Hydraulics of Denil Fishways [J]. *Journal of Hydraulic Engineering*, 1984, 110(9), 1219-1233.

[25] Smagorinsky, J. GENERAL CIRCULATION EXPERIMENTS WITH THE PRIMITIVE EQUATIONS [J]. *Monthly Weather Review*, 1963,91.

[26] Hirt, C. W., Nichols, B. D. Volume of fluid (VOF) method for the dynamics of free boundaries [J]. *Journal of Computational Physics*, 1981, 39(1), 201-225.

[27] Celik, I. B., Cehreli, Z. N., Yavuz, I. Index of Resolution Quality for Large Eddy Simulations [J]. *Journal of Fluids Engineering*, 2005,127(5), 949-958.

[28] Liu, C., Gao, Y., Tian, S. et al. Rortex A New Vortex Vector Definition and Vorticity Tensor and Vector Decompositions [J]. *Physics of Fluids*, 2018, 30(3).

[29] Liu, C. Letter: Galilean invariance of Rortex [J]. *Physics of Fluids*, 2018,30(11), 111701.

[30] Gao, Y., Liu, C. Rortex and comparison with eigenvalue-based vortex identification criteria [J]. *Physics of Fluids*, 2018,30(8), 085107.

[31] Tian, S., Gao, Y., Dong, X. et al. Definitions of vortex vector and vortex [J]. *Journal of Fluid Mechanics*, 2018, 849, 312-339. https://doi.org/10.1017/jfm.2018.406